Biomaterials Science

Accepted Manuscript

This article can be cited before page numbers have been issued, to do this please use: X. Lei, L. Qiu, M. Lan, X. Du, S. Zhou, P. Cui, R. Zheng, P. Jiang, J. Wang and J. Xia, *Biomater. Sci.*, 2020, DOI: 10.1039/D0BM01467B.

ROYAL SOCIETY OF CHEMISTRY

rsc.li/biomaterials-science

View Article Online
DOI: 10.1039/D0BM01467B

ARTICLE

Antibacterial photodynamic peptides for staphylococcal skin infection

Received 00th January 20xx,
Accepted 00th January 20xx

DOI: 10.1039/x0xx00000x

Xiaoling Lei[a, #], Lin Qiu[a, #], Min Lan[a], Xuancheng Du[c], Shuwen Zhou[a], Pengfei Cui[a], Ronghui Zheng[a], Pengju Jiang*[a], Jianhao Wang*[a,d], Jiang Xia*[b]

As the barrier between the human body and the outside world, the skin is vulnerable to pathogenic microorganisms, especially at the condition of skin injuries such as burns. Staphylococcus aureus remains the most common type of bacteria that infect humans, and the surging drug resistance poses a major threat to the treatment of these infections. Here we report the development of antibacterial photodynamic peptides (APPs), that are constructed based on the covalent conjugation of an antibacterial peptide and the photosensitizer chlorin e6 (Ce6). Peptide conjugation significantly increases the photo stability of Ce6, while retaining its ROS generation capability under photo irradiation. The APPs combine the antibacterial activity of the peptide and the photodynamic therapy of Ce6, and under the assistance of a mild laser irradiation, can eradicate bacterial infection and inhibits the formation of bacterial biofilms ex vivo. One of the APPs, $(GKRWWKWWRR)_2KGGK(Ce6)G$, AMP_2-Ce6, with Ce6 conjugated with the dimeric peptide, showed exceptional antibacterial activity with MIC_{90} value around 3.2 μM without photo irradiation and < 0.1 μM with a short light treatment. Supported by a hydrogel matrix composed of gelatin and recombinant human collagen Ⅲ protein (rhCol Ⅲ) mimicking the extracellular matrix of the skin cells, AMP_2-Ce6 efficiently accelerated the healing rate of wounds and improved the quality of wound healing in mice infected with Staphylococcus aureus. Altogether, here we report the development of antibacterial photodynamic peptides, which together with a regenerative matrix material exhibit an added effect against Staphylococcal skin infection. This composite material holds promise as a new type of wound dressing materials for skin infection and wound healing.

Introduction

The Gram-positive commensal bacterium *Staphylococcus aureus* (*S. aureus*) colonizes the anterior nares and other anatomic sites of approximately one third of the human population [1,2]. *S. aureus* can infect almost any body site and cause *S. aureus* skin and soft tissue infections (SSTI). *S. aureus* infection is now a leading cause of food-borne illness, the second leading cause of infectious endocarditis [3], and an important cause (~2%) of all hospital admissions [4].

Infections through the skin are a serious problem in burn surgery or any other types of skin damage [5–9]. The skin acts as a natural protective barrier for the human body, which protects tissues and organs from physical and chemical stimuli, and pathogenic microorganisms. Skin injury is often associated with a high risk of bacterial infection. In the wound healing process, the stages of hemostasis, inflammation, proliferation and remodeling are all carried out in an orderly manner. Bacterial infection disturbs these steps of skin repair and the delayed wound healing in turn causes persistent infection at the wound site, leading to deterioration of the infection. Among all the bacterial skin infections, Staphylococcal skin infection remains the most common one.

Antimicrobial resistance has been the major challenge of the treatment of Staphylococcal infection. Antibiotic-resistant *S. aureus* emerged soon after the clinical use of β-lactam antibiotics penicillin and methicillin [10]. Recently, *S. aureus* became a major threat to the human health [11–14], which accounted for nearly 60% of all *S. aureus* isolates recovered from hospital intensive care units [15]. Unfortunately, accompanying the rise in global resistance is a setback in antibacterial drug discovery, including shortages of new mechanisms and new targets in recent years. Therefore, the crisis of antibacterial resistance calls for new mechanisms that are significantly different from the existing ones.

Many exogenous sterilization strategies have been reported to combat drug resistance, including light-stimulated [16-24], ultrasound-stimulated and microwave-stimulated sterilization methods [25-28]. Antibacterial photodynamic therapy (APDT) has emerged as a new type of antibacterial treatments and holds promise towards combating drug resistance [29]. APDT utilizes non-toxic photosensitizers (PSs) under light irradiation, typically in the visible wavelength range (400-700 nm) to generate reactive oxygen species (ROS) or reactive transients to induce oxidative stress in bacterial cells and eventually cell death [9,30]. The PS molecules are

[a.] *School of Pharmacy, Changzhou University, Changzhou, Jiangsu 213164, China.*
[b.] *Department of Chemistry, the Chinese University of Hong Kong, Shatin, Hong Kong SAR, China.*
[c.] *Institute of Advanced Interdisciplinary Science, School of Physics, Shandong University, Jinan 250100, China.*
[d.] *Changzhou Le Sun Pharmaceuticals Co., Ltd, Changzhou, Jiangsu 213125, China*
*Corresponding Author: pengju.jiang@gmail.com; Jianhao Wang, minuswan@163.com; Jiang Xia, jiangxia@cuhk.edu.hk.
#These authors contributed equally to this work.
Electronic Supplementary Information (ESI) available: Supplementary figures. See DOI: 10.1039/x0xx00000x

divided into two types based on the ROS molecules that they generate: hydroxyl radical (type I) and singlet oxygen (type II). Compared with traditional antibiotics, APDT can solve the drug resistance as no resistance has been developed against PSs, even after repeated treatment with APDT [31]. Several reasons may account for this property. First, the short lifetime of the ROSs precludes the development of resistance. Second, the low dark toxicity of the RSs does not elicit adaptive survival mechanism in bacteria. Third, PDT treatment normally severely damages the cells, disabling them to confer cross-generation adaptivity. Fourth, the ROS normally damage cells structures and multiple metabolic pathways, instead of a single site [32]. These features make APDT molecules ideal candidates to combat resistant bacterial strains.

Because of the ROS are short-ranged and non-selective bactericidal agents, targeted delivery of the PS to the pathogenic bacteria is the key towards high antibacterial efficacy and low side effects. Antibacterial peptides exhibit their bactericidal effect by first binding to the bacterial cells before breaking up the cell wall [33–35]. We reason that covalent conjugation of antibacterial peptide with a selected PS molecule will facilitate the effective enrichment of PS inside or on the membrane of bacterial cells. Further, the antibacterial activity of the peptide will enhance the APDT effect. We therefore design and synthesize antibacterial photodynamic peptides (APPs), embed the APPs in a regenerative hydrogel composed of gelatin and recombinant type Ⅲ collagen, and demonstrate the antibacterial and skin regeneration activity in staphylococcal skin infection *in vivo* (Figure 1).

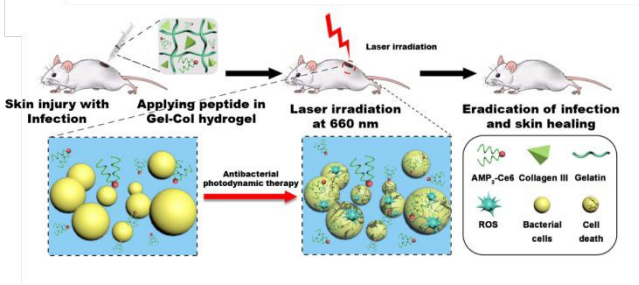

Figure 1. Schematic illustration of the antibacterial photodynamic therapy to treat staphylococcal skin infection and skin injury in a mouse model. The antibacterial photodynamic peptide (AMP_2-Ce6) was applied to the infected skin wound by a Gel/Col hydrogel.

Experimental Section

Material

2-(1H-benzotriazol-1-yl)-1,1,3,3-tetramethyluronium hexafluorophosphate (HBTU), Fmoc-protected amino acids, Rink Amide-MBHA resin and N-hydroxybenzotriazole (HOBt) were obtained from GL Biochemical Ltd (Shanghai, China). Recombinant human collagen Ⅲ was purchased from Jiangsu Yuezhi Biopharmaceutical, Ltd. (collagen content > 90%, batch number: 20180823). N-(3-(dimethylamino)-propyl-N'-ethylcarbodiimide) hydrochloride (EDC), phosphate-buffered saline (PBS buffer), Luria–Bertani broth medium (LB), and 3-(4,5-dimethyl-2-thiazolyl)-2,5-diphenyl-2-H-tetrazolium bromide (MTT reagent) were obtained from Sigma-Aldrich. Chlorin e6 (Ce6) was purchased from J&K Chemical Ltd. DCFH-DA fluorescent probe and live/dead bacterial viability kits were purchased from Thermo Fisher Scientific. All other chemicals were obtained from Adamas-beta and used without further purification. Deionized (DI) water (Millipore Milli-Q grade, 18.2 MΩ) was used in all experiments. The UV-vis absorption was monitored using a UV-vis spectrophotometer (UV-3600, Shimadzu).

Preparation and characterization of AMP_2-Ce6

AMP_2 was synthesized by solid phase peptide synthesis technique based on the 9-fluorenylmethoxycarbonyl (Fmoc) chemistry using Rink Amide-MBHA resin, and a 5-fold excess of amino acid activated by one equivalent of 1:1 HBTU/HOBt in DMF. Each coupling lasted 30 min. The Fmoc group was deprotected by piperidine/DMF (20%, v/v) during 30 min. Fmoc-Lys(Fmoc)-OH was used for the synthesis of the fifth amino acid and Fmoc-Lys(Mtt)-OH was used for the synthesis of the second amino acid. After the sequence was synthesized, Mtt group was cleaved off by TFA/TIS/DCM (1:5:94, v/v/v) and the released amino group was then coupled with 5-fold excess of free Ce6 in the presence of DIPEA activated by 1:1 EDC/HOBt in DMF. AMP_2-Ce6 was cleaved from the resin by a cleavage cocktail of TFA, EDT, water, and TIS (94:2.5:2.5:1, v/v/v/v) for 3 h at room temperature. It was then precipitated in ice-cold diethyl ether, pelleted by centrifugation, dissolved in water, and purified by HPLC (Shimadzu, Kyoto, Japan). Solvent A was 0.1% (v/v) TFA in water, and solvent B was 0.1% (v/v) TFA in acetonitrile. A linear gradient of increasing percentage of solvent B was set. Flow rate was set at 1 mL/min. Peptide peaks were detected at 220 nm and 664 nm. Preparative HPLC was performed on a Vydac (218TP510) RP-HPLC column with a flow rate of 3 mL/min. The identity of AMP_2-Ce6 was confirmed by LC-MS: m/z was calculated for $[M+6H]^{6+}$ 681.46, found 681.36. AMP-Ce6 and AMP_4-Ce6 were synthesized using similar method.

Preparation of gelatin based composite hydrogel Gel-Col@AMP_2-Ce6

First, 1 g of gelatin was dissolved in 10 mL of DI water, heated to 40°C and stirred for 30 min, and collagen Ⅲ was added to the mixture. Then, the prepared AMP_2-Ce6 was added to the above mixed solution. The prepared 10% transglutaminase aqueous solution was added into gelatin-collagen Ⅲ mixture for enzyme cross-linking 3 min. The prepared composite gelatin solution was put into the mold and stood for 30 min to form a gel.

Singlet oxygen generation from the AMP_2-Ce6

DCFH-DA fluorescent probe was used to investigate the singlet oxygen generation capability of the AMP_2-Ce6. In brief, AMP_2-Ce6 was irradiated using a NIR laser (660 nm, 0.8 W/cm^2) for 6 min, and then 10 μL of DCFH-DA (100 μM) was added. The generation of singlet oxygen from the AMP_2-Ce6 could be quantitatively assessed by the analysis of the fluorescence spectrum of DCF. On the basis of this experiment, in order to explore the influence of irradiating time on ROS, we set different irradiate time (0, 2, 4, 6, 8, 10, 12, 14 min) to irradiate the sample. The fluorescence was monitored using multifunctional microplate reader (Spark, Tecan).

Bacteria culture

Pathogenic bacteria of *Staphylococcus aureus* (*S. aureus*, ATCC 6538) was employed in our experiments. The bacteria were cultured in LB medium and harvested at the exponential growth phase via centrifugation. The bacteria concentration could be monitored photometrically by measuring the optical density (OD) at a

wavelength of 600 nm. The OD_{600} values of the bacteria stock solutions were re-adjusted to 0.1 before the experiments, which corresponded to concentrations of 1×10^8 CFU per mL for *S. aureus*, respectively, calculated based on the gold standard colony counting method.

In vitro photodynamic antimicrobial activity of the AMP_2-Ce6

250 μL of AMP_2-Ce6 (4 μM) was mixed with 1 mL *S. aureus* culture (10^7 CFU/mL) and incubate for 1 h. Then, the mixture of *S. aureus* and AMP_2-Ce6 was irradiated with a NIR laser (660 nm, 0.8 W/cm^2) for 6 min, and the antibacterial performance of AMP_2-Ce6 was evaluated by the bacteria culture and the determination of the minimum inhibitory concentration. In addition, the antimicrobial assay of AMP_2-Ce6 was performed in 96-well plate. Briefly, AMP_2-Ce6 (4 μM) was incubated with *S. aureus* LB solutions (10^5 CFU/mL) on 96 well plates at 37 °C and the OD_{600} values of the mixture at different time intervals was measured. The *S. aureus* LB solution (10^5 CFU/mL) without the AMP_2-Ce6 incubation was used as the control.

AMP_2-Ce6 for Biofilm Formation Inhibition

First, *S. aureus* (10^6 CFU/mL) and AMP_2-Ce6 (4 μM) were added to the 96-well plate. After 48 h incubation, the plates were gently washed by PBS three times, and 300 μL of 1% (v/v) crystal violet ethanol solution was added and reacted for 15 min. The plates after crystal violet staining were then imaged by camera, and the corresponding absorbance of crystal violet solution at 590 nm was also measured to investigate the ability of AMP_2-Ce6 for biofilm formation inhibition.

SEM-based morphology studies of bacteria

For the SEM-based bacterial morphology study, mixtures of *S. aureus* and the AMP_2-Ce6 before and after NIR laser irradiation were dropped onto silicon wafers, respectively, fixed by glutaraldehyde (2%). Then, the samples were dehydrated with a series of ethanol solutions (50%, 70%, 90%, and 100%) for 10 min at each step. After ethanol dehydration, the silicon wafers with bacteria were dried by nitrogen and imaged with SEM (S-4700, Hitachi) after platinum sputter-coating.

SEM-based morphology studies of hydrogels

The morphology of Gelatin, Gel-Col and Gel-Col@AMP_2-Ce6 hydrogels were examined by SEM. First, the prepared hydrogel is freeze-dried, and the surface is cut off with liquid nitrogen. Then, the hydrogels were completely dried by nitrogen and imaged with SEM (TM3030plus, Hitachi).

Live/Dead Bacterial Staining Analysis

The viability of the bacteria was investigated by the live/dead bacteria staining assay. Briefly, the bacteria treated with AMP_2-Ce6 before and after irradiation were mixed with the dye solution containing 1 μM SYTO 9 and 1 μM PI at room temperature for 20 min, and then imaged by confocal microscopy (LSM710, Carl Zeiss). PBS was used as the control. According to the manufacturer's instructions, live bacterial cells were stained by SYTO 9 dye (green color) while dead bacterial cells were labelled by PI (red color) due to damaged cell wall and membrane.

Cytotoxicity of the AMP_2-Ce6

The cytotoxicity of the AMP_2-Ce6 was assessed with mouse fibroblasts (L929) based on the MTT assay. First, L929 cells seeded on 96-well microplates (10^4 cells per well) were grown overnight and treated with the AMP_2-Ce6 with different concentrations (0, 0.5, 1, 2, 4, 8, or 16 μM), respectively. After 24 h of incubation, the MTT assay was carried out, and the viability of the L929 cells was investigated by measuring the absorbance at 490 nm with a microplate reader.

Mouse wound model of *S. aureus* infection

Female mice (Balb/c, 6 weeks, ~20 g) were purchased from the Changzhou Cavens Biological Technology Co, Ltd., and allowed to acclimatize for 1 week in the laboratory. All animal procedures were in accordance with permission from the Shandong University Animal Experiment Ethics Review and the Health Guide for the Care and Use of Laboratory Animals of National Institutes. To construct the infected mouse wound model, the mice were anesthetized and an oval full-thickness wound (10 mm in long axis) extending through the panniculus carnosus was first created in the upper back of diabetic mouse using disposable biopsy punch and was then inoculated with bacteria (10^7 CFU/mL of *S. aureus*) for 2 days *in situ*.

In vivo therapy of *S. aureus*-infected wounds

The above-mentioned mice with *S. aureus* infection wounds were divided into seven treatment groups, each group contained five mice. These treatment groups included PBS, Gelatin, AMP_2-Ce6, AMP_2-Ce6/Irradiation, Gel-Col, Gel-Col@AMP_2-Ce6, and Gel-Col@AMP_2-Ce6/Irradiation. Here, NIR irradiation (660 nm, 0.8 W/cm^2, 6 min) was employed. In order to eliminate bacteria from *S. aureus*-infected wounds in vivo and promote wound healing, the hydrogel systems were applied onto the surface of infected wounds, and the wounds were photographed every day to record their healed areas. After 10 days of treatment, the mice were executed and the skin tissues at the infected wound sites were dissected from the mice. Bacterial culture, hematoxylin and eosin (H&E) staining, Masson's trichrome staining, and immunohistochemistry CD31 staining of the dissected skin tissues were subsequently conducted to evaluate the actual efficacy of hydrogel systems for eliminate bacteria from *S. aureus*-infected wounds in vivo and promote wound healing.

Results and Discussion

Design and synthesis of antibacterial photodynamic peptides(APPs)

The antibacterial peptide, known as Tet213 (KRWWKWWRR) was identified through chemoinformatics and machine learning by Fjell et al [36]. There are many factors affecting the antibacterial activity of antimicrobial peptides [37-39]. The antibacterial activities were found to be comparable or superior to those of conventional antibiotics and existing peptides against a broad array of multi-resistant human pathogens [40–43]. Here we synthesized APPs by covalently conjugating Ce6 with the selectively deprotected peptide sequence through solid phase peptide synthesis on resin. Three variants of APPs were synthesized, AMP-Ce6, AMP_2-Ce6 and AMP_4-Ce6, each containing a monomer, dimer or tetramer of Tet213 and one Ce6 molecule respectively (Figure 2A). When Ce6 is conjugated to AMP_2, there are absorption peaks at both 403 nm and 664 nm, proving that Ce6 has been successfully conjugated with AMP_2 (Figure 2B). The UV-Vis absorption of Ce6 significantly decreases at 403 nm and 664 nm after photo irradiation at 660 nm for 6 min, indicating that Ce6 has low photo stability (Figure 2C). In contrast, the UV-Vis

View Article Online
DOI: 10.1039/D0BM01467B

absorption spectrum of peptide conjugate AMP_2-Ce6 did not change after photo irradiation (Figure 2D), indicating covalent conjugation of Ce6 with the peptide sequence significantly improved the photo stability of Ce6. Fluorescence spectrum of AMP_2-Ce6 also indicated the successful conjugation of Ce6 with AMP_2 (Figure S1).

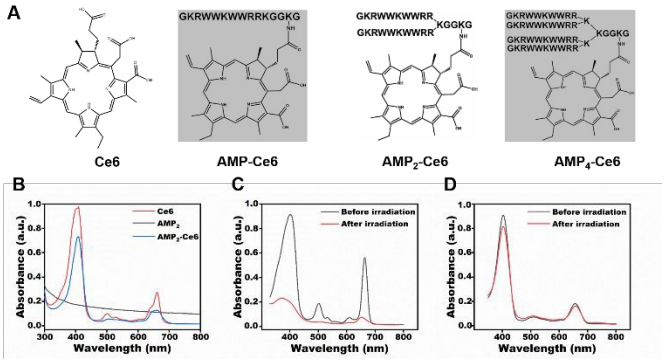

Figure 2. Structures and absorption spectra of antibacterial photodynamic peptides. (A) The chemical structures of AMP-Ce6, AMP_2-Ce6, and AMP_4-Ce6. As Ce6 contains three carboxylic acids, shown here are the most probable conjugation products. (B) UV-vis absorption spectra of Ce6, AMP_2 and AMP_2-Ce6 without photo irradiation. (C, D) Changes of absorption spectra of free Ce6 molecules (C) and AMP_2-Ce6 (D) before and after NIR laser (660 nm, 0.8 W/cm^2) irradiation for 6 min.

Bactericidal activity of the APPs ex vivo

We next evaluated the bactericidal activities of the APPs. In the absence of photo irradiation, after 1 h incubation, the peptides showed a dose-dependent activity to kill *S. aureus* culture (Figure 3A-3C). AMP_2-Ce6 shows the highest activity, with MIC_{50} and MIC_{90} being 0.4 μM and 3.2 μM respectively, both lower than those of AMP-Ce6 (MIC_{50}=9 μM, MIC_{90}=18 μM) and AMP_4-Ce6 (MIC_{50}=12 μM, MIC_{90}=20 μM). Coupling Ce6 did not affect the activity of AMP_2 (Figure S2). Based on the corresponding standard curves shown in Figures S3, the release curves of loaded Ce6 in which the cumulative release amounts of Ce6 were obtained (Figure S4). It was found that Ce6 can produce singlet oxygen under laser irradiation, oxidative damage to bacterial cell structure, resulting in bacterial death (Figure S5).

We next evaluated the photodynamic bactericidal activity of the APPs again *S. aureus*. Starting from a *S. aureus* culture of 10^7 CFU, the peptides were mixed with the bacterial culture for 1 h and irradiated with NIR laser (660 nm, 0.8 W/cm^2) for 6 min, before the colony forming units were counted. The first screening experiment shows that at 4 μM, AMP_2-Ce6 can eradicate *S. aureus* cells after 1 h incubation, whereas AMP-Ce6 and AMP_4-Ce6 were not able to completely kill all the cells. 6-min irradiation by NIR can markedly increase the bactericidal activities of all three APPs (Figure 3D). And the bactericidal activity of AMP_2-Ce6 under different concentrations of laser irradiation showed that the MIC_{90} value of AMP_2-Ce6 after irradiation treatment was < 0.1 μM (Figure 3E).

We next measured the generation of reactive oxygen species (ROSs) inside *S. aureus* cells in the presence and absence of photo irradiation using a DCFH-based assay. ROSs were detected with the fluorescent probe DCFH-DA. DCFH-DA has no fluorescence and can pass through the cell membrane freely. After entering the cell, it can be hydrolyzed by intracellular esterase to produce DCFH which will retain inside the cell. Intracellular ROS molecules can oxidize the non-fluorescent DCFH to produce fluorescent DCF; the level of DCF thereby provides a measure of the amount of ROS produced inside the cell. We observed that the amount of ROS species of peptide conjugated Ce6 is comparable as free Ce6 (Figures 3F). Increasing the photo irradiation time indicates that at a photo density of 0.8 W/cm^2, after 4 min the increase of ROS species gradually plateaued (Figure 3G). Next, the cell morphological change was examined by scanning electron microscopy (SEM) (Figure 4). Normal *S. aureus* cells have smooth bodies, while cellular deformation and surface collapse was observed after AMP_2-Ce6 incubation and irradiation, indicating severe disruption of the bacterial cell wall and membrane.

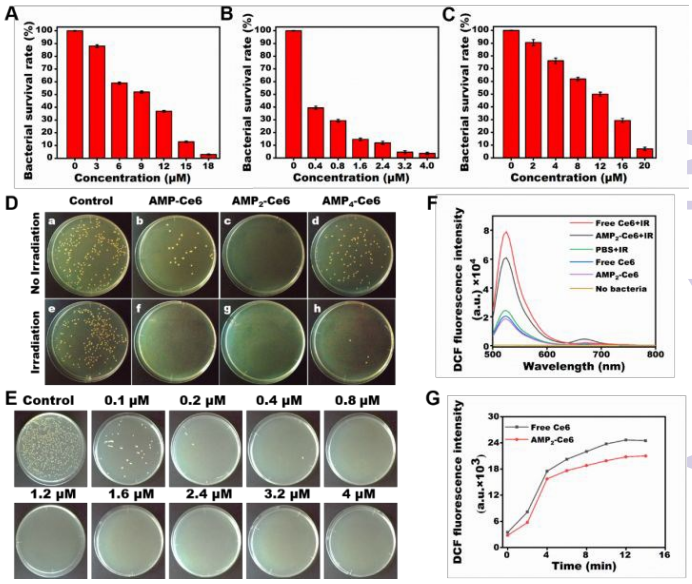

Figure 3. Bactericidal activities of the APPs against *S. aureus*. (A, B, C) Antibacterial activity of the three peptides in the absence of photo irradiation. The bacterial numbers were calculated as CFU, and normalized. (D) Bactericidal activities of the three peptides with or without laser irradiation. Similarly, peptides at 20 μM in 50 μL were mixed with 1 mL *S. aureus* culture for 1 h and then photo irradiated for 6 min (660 nm, 0.8 W/cm^2). 100 μL cultures were then plated and colonies were counted after 12 h. (E) Bactericidal activity of AMP_2-Ce6 with laser irradiation at different concentration. MIC_{90}< 0.1 μM. (F) Detection of the increased ROS upon peptide treatment. Fluorescence spectra of DCFH-DA in AMP_2-Ce6 solution before and after NIR laser irradiation. (G) Detection of ROS generation of AMP_2-Ce6 upon different photo irradiation times. Peptide at 20 μM in 250 μL was mixed with 1 mL *S. aureus* culture for 1 h and then photo irradiated for different time (660 nm, 0.8 W/cm^2).

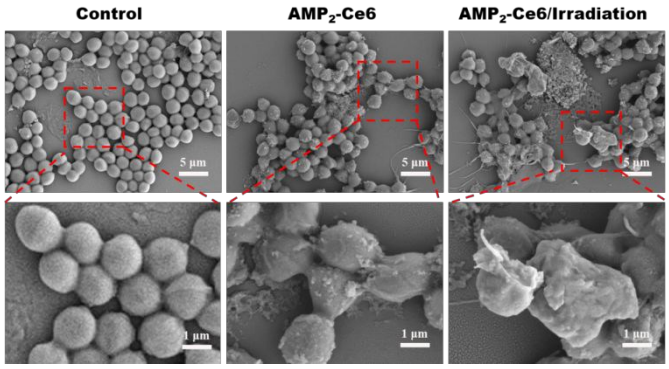

Figure 4. Representative SEM images of *S. aureus* incubated with AMP_2-Ce6 before and after NIR laser irradiation (660 nm, 0.8 W/cm^2, 6 min), PBS was used as the control.

Bacterial growth inhibition

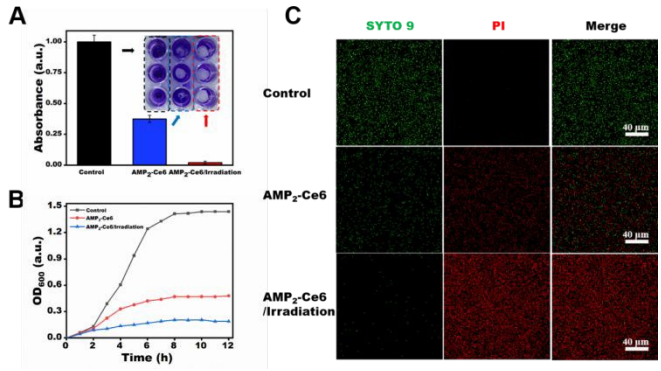

Figure 5. Antibacterial activity *ex vivo*. (A) Crystal violet staining images and corresponding absorbance for integrated *S. aureus* biofilm incubated with the AMP_2-Ce6. The biofilm without incubation with the AMP_2-Ce6 was used as the control. (B) Growth curves of *S. aureus* incubated with AMP_2-Ce6. The growth of *S. aureus* without AMP_2-Ce6 incubation was used the control. (C) Representative overlapping fluorescence images for the live/dead staining assay of *S. aureus* incubated with AMP_2-Ce6 before and after NIR laser irradiation.

We then next used a crystal violet staining assay to explore whether the APPs can inhibit the formation of biofilm [44]. Co-incubation of AMP_2-Ce6 with *S. aureus* for 2 days significantly inhibited the formation of biofilm in the absence of photo irradiation (Figure 5A, Figures S6). Also the presence of AMP_2-Ce6 significantly inhibited the growth of bacterial culture (peptide concentration at 4 μM and the bacterial culture started at 10^6 CFU/mL). When the bacterial culture was by a one-time, 6-min, laser irradiation at time zero, the bacterial growth was nearly completely inhibited (Figure 5B). This indicates that combining photodynamic activity and the activity of the peptide results in effective suppression of the cell growth, suggesting a prolonged bacterial growth inhibition effect in the clinical settings. Utilizing SYTO 9 (green) and PI (red) dyes, we showed that after co-incubation of AMP_2-Ce6 (4 μM) with *S. aureus* for 30 min, half of the bacterial cells have died (red) in the absence of photo irradiation. If this procedure was combined with a 10-min laser irradiation (660 nm, 0.8 W/cm^2), the majority of the *S. aureus* cells have died (Figure 5C). Altogether these data show that the APP AMP_2-Ce6 has a remarkable bactericidal effect, and can significantly inhibit biofilm formation and growth profile, and induce cell death of *S. aureus*. The peptide also showed minimal toxicity to cells (Figure S7).

Treatment of staphylococcal skin infection *in vivo*

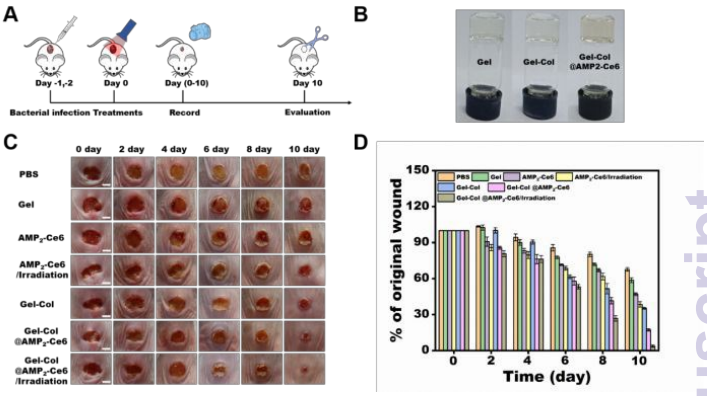

Figure 6. Treatment of staphylococcal skin infection *in vivo.* (A) Scheme illustration of the procedures including the establishment of *S. aureus* infection mice model and subsequent treatment regime. (B) Representative photographs of Gelatin, Gel-Col, and Gel-Col@AMP_2-Ce6 hydrogel. (C) Representative photographs of wounds infected with *S. aureus* in seven different treatment groups (PBS, Gelatin, AMP_2-Ce6, AMP_2-Ce6/Irradiation, Gel-Col, Gel-Col@AMP_2-Ce6, Gel-Col@AMP_2-Ce6/Irradiation) within 10 days. NIR laser irradiation (660 nm, 0.8 W/cm^2, 6 min) was employed. (D) Quantification of the areas of infected wounds of mice shown in (C). The values of wound healing ratios (% of original wound) represent the mean from three independent experiments, and the error bars indicate the SD from the mean.

To apply AMP_2-Ce6 to the damaged and infected skin, a dressing material is needed to allow the soluble peptide to stay on the surface of the skin without being dried out. For this purpose, we developed a hybrid gelatin-collagen hydrogel material and checked by SEM (Figure S8). Gelatin and recombinant type Ⅲ collagen protein were crosslinked by transglutaminase to form a gel material. This gel material mimics extracellular matrix of the skin cells, and provides a promotive material to promote skin regeneration and wound healing. Mice with an oval full-thickness wound (10 mm in long axis) extending through the panniculus carnosus in the back, and *S. aureus* infection in the wound were established as an animal model of staphylococcal skin infection (Figure 6A). 7 groups of treatments were established, including PBS, Gelatin, AMP_2-Ce6 without photo irradiation, AMP_2-Ce6 with photo irradiation, Gel-Col hydrogel only, Gel-Col@AMP_2-Ce6 hydrogel without photo irradiation, and Gel-Col@AMP_2-Ce6 hydrogel with photo irradiation. In groups with photo irradiation, the mice were treated by laser for 6 min each day. Over a course of 10 days, both groups 6 and 7 (Gel-Col@AMP_2-Ce6 hydrogel without and with laser irradiation respectively) showed significantly faster wound healing (Figure 6B and 6C). Group 7, Gel-Col@AMP_2-Ce6 hydrogel with laser irradiation showed the most outstanding recovery of the wound. This experiment shows that the antibacterial treatment coincides with the wound healing process, and the antibacterial photodynamic treatment combined with a regeneration-promoting hydrogel material successfully stimulated wound healing.

View Article Online DOI: 10.1039/D0BM01467B

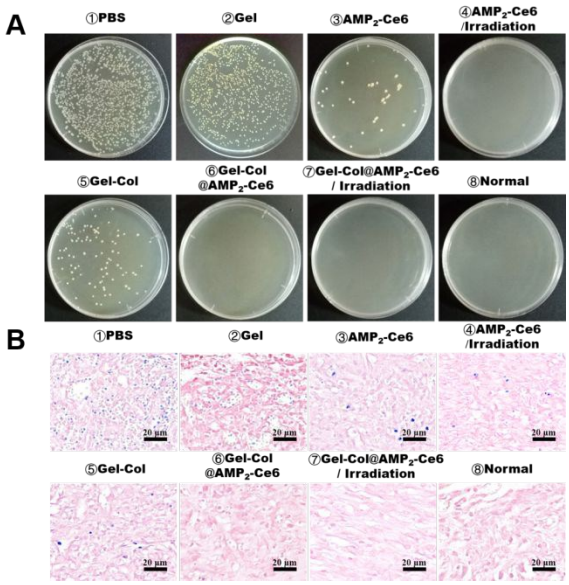

Figure 7. Representative photographs of bacterial cultures from the skin tissues of mice wounds infected with *S. aureus* (A) and the corresponding gram-staining images of the skin tissues of *S. aureus* infected mice wounds (B) in eight different groups (PBS, Gelatin, AMP_2-Ce6, AMP_2-Ce6/Irradiation, Gel-Col, Gel-Col@AMP_2-Ce6, Gel-Col@AMP_2-Ce6/Irradiation, and normal control) on the 10th day of treatment.

We next counted the number of colony forming bacterial cells at the wound sites on day 10. The mice were dissected and the skin areas were crushed evenly with a mortar, and diluted with PBS for bacterial coating experiment. Consistent with the wound healing results, groups 6 and 7 showed complete eradication of the bacteria on the plates (Figure 7A). Also gram-staining of the skin tissue sections supports this conclusion as no signs of the Gram positive bacterial cells were observed in group 7 samples (Figure 7B). This result suggests that wound healing and antibacterial treatment are inseparable.

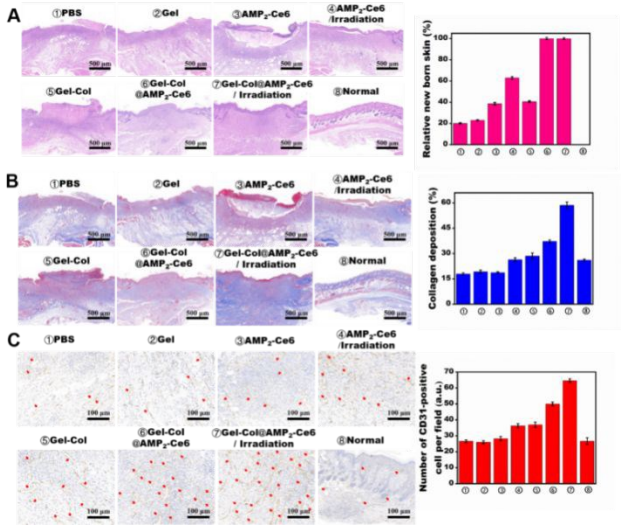

Figure 8. Histological analysis of the wound areas. (A) Representative histological (H&E staining) images and the corresponding quantitative data of new born percentage of the skin tissues of *S. aureus* infected mice wounds in eight different groups on the 10th day of treatment. (B) Representative Masson's trichrome staining images and the corresponding quantitative data of collagen deposition percentage of the skin tissues of *S. aureus* infected mice wounds in eight different groups on the 10th day of treatment. (C) Representative CD31 staining images and the corresponding quantitative data of the CD31-positive cell's number of the skin tissues of *S. aureus* infected mice wounds indicate the condition of blood vessel formation in eight different groups. The values of CD31-positive cell's number were determined on the basis of staining images from three independent experiments. (The red arrows in the images indicated the condition of blood vessel formation in eight different treatment groups).

Next we examined the histological staining of the wound repair and skin regeneration. Notably, H&E staining shows complete re-epithelialization was observed in group 7 only, but not in other groups (Figure 8A). Masson's trichrome staining shows the highest deposition of newly generated collagen in the skin tissues of *S. aureus* infected mice wounds in group 7, reaching up to 59.0 ± 2.0% (Figure 8B). The number of CD31-positive cells is also significantly higher in group 7 than that of any other groups, indicating successful blood vessel formation in this group (Figure 8C). This treatment also showed minimal toxicity to the animals based on the histological analysis of the major organs (Figure S9). Taken together, the combination of APPs and the Gel-Col hydrogel provides a promoting environment for both wound healing and eradication of bacterial infection.

Conclusions

Altogether, we discovered one APP, AMP_2-Ce6 shows exceptionally high antibacterial activity ex vivo, and together with a composite hydrogel system composed of gelatin and recombinant type Ⅲ human collagen, antibacterial photodynamic therapy successfully battled *S. aureus* infection and promoted wound healing in vivo. Both gelatin and type Ⅲ collagen can promote cell adhesion and induce cell proliferation and differentiation. Gelatin-collagen-based hydrogel dressing mimics the extracellular matrix, offers superior permeability and moisture, provides a regenerative environment for the skin cells, and accelerates the wound healing. The hydrogel also serves as a scaffold for cell growth, collagen deposition and new blood vessel formation. Our results show that a combination of an APP, AMP_2-Ce6 and Gel-Col hydrogel together with a mild laser irradiation promotes wound healing, eradicates bacterial infection, and confers minimal toxicity to the skin tissue.

Antibacterial photodynamic therapy is an effective therapy to treat skin infection. One of the limitations is that the laser irradiation may cause damage to the healthy skin tissues around the infection area. Therefore, we chose a low-power NIR source at 660 nm with an intensity of 0.8 W/cm^2 for the animal experiments, and we also use NIR camera to monitor the temperature of the infection site to avoid burning damage to the skin. We observed that during the experiments, the temperature of tissue at the laser irradiated sites did not exceed 42 °C, indicating this treatment is a potentially safe therapy for skin infection.

Conflicts of interest

There are no conflicts to declare.

Acknowledgements

We are grateful for the funds supported by Jiangsu Key Research and Development Plan (Society Development, No. BE2018639), the International Scientific Cooperation Project of Changzhou Scientific Bureau (No. CZ20190009), the Science & Technology Support Program of Changzhou (Application Basic Research, No. CJ20190033), and the QingLan Project of Jiangsu Province. This work was partially funded by the University Grants Committee of Hong Kong (GRF Grants N_CUHK422/18), and a CUHK RSFS grant.

Notes and references

1 C.B. Creech, D.N. Al-Zubeidi and S.A. Fritz, *Dis. Clin. North Am.*, 2015, **29**, 429-464.
2 H.F.L. Wertheim, D.C. Melles, M.C. Vos, W. van Leeuwen, A. van Belkum, H.A. Verbrugh and J.L. Nouwen, *The Lancet Infect. Dis*., 2005, **5**, 751-762.
3 J.J. Weems, *Postgrad. Med.*, 2001, **110**, 24-36.
4 J.A. Lindsay and M.T.G. Holden, *Trends Microbiol.*, 2004, **12**, 378-385.
5 F. Ibrahim, T. Khan and G.G.A. Pujalte, *Prim. Care*, 2015, **42**, 485-499.
6 A. Russo, E. Concia, F. Cristini, F.G. de Rosa, S. Esposito, F. Menichetti, N. Petrosillo, M. Tumbarello, M. Venditti, P. Viale, C. Viscoli and M. Bassetti, *Clin. Microbiol. Infec.*, 2016, **22**, S27-S36.
7 P.B. Hill and A. Imai, *Comp. Immunol. Microbiol. Infect. Dis.*, 2016, **49**, 8-28.
8 D.L. Stulberg, A.M. Penrod and R.A. Blatny, *Am. J. Med.*, 2002, **66**, 119-124.
9 J. Wang, X.-Y. Chen, Y. Zhao, Y. Yang, W. Wang, C. Wu, B. Yang, Z. Zhang, L. Zhang, Y. Liu, X. Du, W. Li, L. Qiu, P. Jiang, X.-Z. Mou and Y.-Q. Li, *ACS Nano*, 2019, **13**, 11686-11697.
10 F.F. Barrett, M.G.R. Jr and M. Finland, *N. Engl. J. Med.*, 1968, **279**, 441-448.
11 F.D. Lowy, *N. Engl. J. Med.*, 1998, **339**, 520-532.
12 J.M. Boyce and W.A. Causey, *Infect. Control*, 1982, **3**, 377-383.
13 M.W. Kline and E.O. Mason, *Pediatr. Clin. N. Am.*, 1998, **35**, 613-624.
14 M.E. Mulligan, K.A. Murray-Leisure, B.S. Ribner, H.C. Standiford, J.F. John, J.A. Korvick, C.A. Kauffman and V.L. Yu, *Am. J. Med.*, 1993, **94**, 313-328.
15 A.R.F. System, *Am. J. Infect. Control*, 2004, **32**, 470-485.
16 J. Li, X. Liu, L. Tan, Z. Cui, X. Yang, Y. Liang, Z. Li, S. Zhu, Y. Zheng, K. W. K. Yeung, X. Wang and S. Wu, *Nat. Commun.*, 2019, **10**, 4490.
17 M. Li, L. Li, K. Su, X. Liu, T. Zhang, Y. Liang, D. Jing, X. Yang, D. Zheng, Z. Cui, Z. Li, S. Zhu, K.W.K. Yeung, Y. Zheng, X. Wang and S. Wu, *Adv. Sci.*, 2019, **6**, 1900599.
18 Q. Zhang, X. Liu, L. Tan, Z. Cui, Z. Li, Y. Liang, S. Zhu, K.W.K. Yeung, Y. Zheng and S. Wu, *Chem. Eng. J.*, 2020, **383**, 123088.
19 Y. Li, X. Liu, L. Tan, Z. Cui, D. Jing, X. Yang, Y. Liang, Z. Li, S. Zhu, Y. Zheng, K.W.K. Yeung, D. Zheng, X. Wang and S. Wu, *Adv. Funct. Mater.*, 2019, **29**, 1900946.
20 X. Xie, C. Mao, X. Liu, L. Tan, Z. Cui, X. Yang, S. Zhu, Z. Li, X. Yuan, Y. Zheng, K.W.K. Yeung, P.K. Chu and S. Wu, *ACS Central Sci.*, 2018, **4**, 724–738.
21 Y. Xiang, C. Mao, X. Liu, Z. Cui, D. Jing, X. Yang, Y. Liang, Z. Li, S. Zhu, Y. Zheng, K. W. K. Yeung, D. Zheng, X. Wang and S. Wu, *Small*, 2019, **15**, e1900322.
22 Y. Li, X. Liu, B. Li, Y. Zheng, Y. Han, D.-F. Chen, K. W. K. Yeung, Z. Cui, Y. Liang, Z. Li, S. Zhu, X. Wang and S. Wu, *ACS Nano*, 2020, **14**, 8157-8170.
23 C. Wang, J. Li, X. Liu, Z. Cui, D.-F. Chen, Z. Li, Y. Liang, S. Zhu and S. Wu, *Biomater. Sci.*, 2020, **8**, 4216-4224.
24 Q. Wu, X. Liu, B. Li, L. Tan, Y. Han, Z. Li, Y. Liang, Z. Cui, S. Zhu, S. Wu and Y. Zheng, *J. Mater. Sci. Technol.*, 2020, **4**, 084
25 K. Su, L. Tan, X. Liu, Z. Cui, Y. Zheng, B. Li, Y. Han, Z. Li, S. Zhu, Y. Liang, X. Feng, X. Wang and S. Wu, *ACS Nano*, 2020, **14**, 2077-2089.
26 Y. Qiao, X. Liu, B. Li, Y. Han, Y. Zheng, K. W. K. Yeung, C. Li, Z. Cui, Y. Liang, Z. Li, S. Zhu, X. Wang and S. Wu, *Nat. Commun.*, 2020, **11**, 4446.
27 D. Sun, X. Pang, Y. Cheng, J. Ming, S. Xiang, C. Zhang, P. Lv, C. Chu, X. Chen, G. Liu and N. Zheng, *ACS nano*, 2020, **14**, 2063-2076.
28 X. Pang, Q. Xiao, Y. Cheng, E. Ren, L. Lian, Y. Zhang, H. Gao, X. Wang, W. Leung, X. Chen, G. Liu and C. Xu, *ACS nano*, 2019, **13**, 2427-2438.
29 F. Cieplik, D. Deng, W. Crielaard, W. Buchalla, E. Hellwig, A. Al-Ahmad and T. Maisch, *Crit. Rev. Microbiol.*, 2018, **44**, 571-589.
30 Y. Liu, R.R. Qin, S.A.J. Zaat, E. Breukink and M. Heger, *J. Clin. Transl. Res.*, 2015, **1**, 140-167.
31 J. Wang, H. Wu, Y. Yang, R. Yan, Y. Zhao, Y. Wang, A. Chen, S. Shao, P. Jiang and Y.-Q. Li, *Nanoscale*, 2018, **10**, 132-141.
32 F.M. Lauro, P. Pretto, L. Covolo, G. Jori and G. Bertoloni, *Photochem. Photobiol. Sci.*, 2002, **1**, 468-470.
33 S. Schastak, S. Ziganshyna, B. Gitter, P. Wiedemann, and T. Claudepierre, *PLoS One*, 2010, **5**, e11674.
34 M. Mahlapuu, J. Håkansson, L. Ringstad and C. Björn, *Front. Cell. Infect. Microbiol*., 2016, **6**, 194.
35 J. Lei and L. Sun, *Am. J. Transl. Res.*, 2019, **11**, 3919-3931.
36 M. Kazemzadeh-Narbat, J. Kindrachuk, K. Duan, H. Jenssen, R.E.W. Hancock and R. Wang, *Biomaterials*, 2010, **31**, 9519-9526.
37 C.D. Fjell, H. Jenssen, K. Hilpert, W. A. Cheung, N. Pante, R.E.W. Hancock and A. Cherkasov, *J. Med. Chem.*, 2009, **52**, 2006-2015.
38 H. Gong, J. Zhang, X. Hu, Z. Li, K. Fa, H. Liu, T.A. Waigh, A. McBain and J.R. Lu, *ACS Appl. Mater. Inter.*, 2019, **11**, 34609-34620.
39 P. Salas-Ambrosio, A. Tronnet, P. Verhaeghe and C. Bonduelle, *Biomacromolecules*, 2020, **7**, 34-45.
40 M. Dathe, M. Schümann, T. Wieprecht, A. Winkler, M. Beyermann, E. Krause, K. Matsuzaki, O. Murase and M. Bienert, *Biochemistry*, 1996, **35**, 12612-12622.
41 L. Wang, J. Chen, L. Shi, Z. Shi, L. Ren and Y. Wang, *Chem. Commun.*, 2014, **50**, 975-977.
42 J. Chen, Y. Zhu, Y. Song, L. Wang, J. Zhan, J. He, J. Zheng, C. Zhong, X. Shi, S. Liu, L. Ren and Y. Wang, *J. Mater. Chem. B*, 2017, **5**, 2407-2415.
43 N. Annabi, D. Rana, E. Shirzaei Sani, R. Portillo-Lara, J.L. Gifford, M.M. Fares, S.M. Mithieux and A.S. Weiss, *Biomaterials*, 2017, **139**, 229-243.
44 G.A. O'Toole and R. Kolter, *Mol. Microbiol.*, 1998, **28**, 449-461.

View Article Online
DOI: 10.1039/D0BM01467B

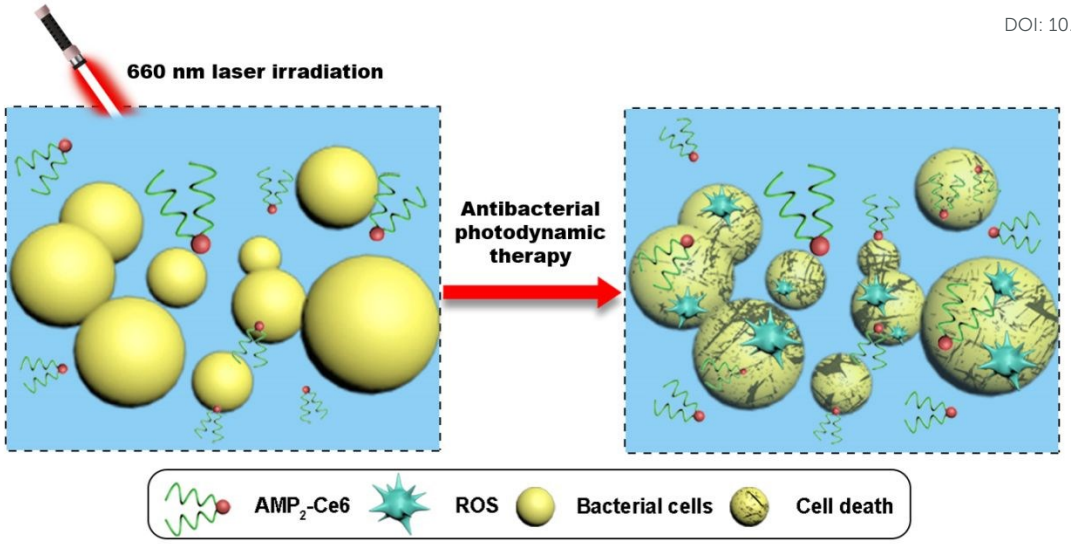

A multicomponent system centered on antibacterial photodynamic peptides and supported by a regenerative gelatin-collagen (Gel-Col) hydrogel.